Control Strategy Optimization of Voltage Source Converter Connected to Various Types of AC Systems

Zehong Liu, *Senior Member*, *IEEE*, and Xianshan Guo

***Abstract*—Connecting the voltage source converters (VSCs) to various types of AC systems results in different operation characteristics and core problems associated with traditional control strategies. Therefore, it is necessary to optimize the control strategies of the VSCs according to the types of AC systems. For the VSCs connected to islanded renewable power plants, a voltage/frequency (*V*/*f*) droop control strategy is proposed to damp fluctuations of AC voltage and frequency in the island, which is vital for bipolar VSC control. In addition, a multi-branch impedance equivalent method for renewable power plants is proposed, with which large-scale renewable power plants can be modeled accurately in the frequency domain to prevent wide-band oscillation. For the VSCs connected to strong AC systems, smart AC voltage and coordinated frequency transient control strategies are proposed, which can improve AC system transient stability. For the VSCs connected to weak AC systems, the relationship between the system stability and strength is analyzed, and then the control strategy of inner-loop control parameter optimization and outer-loop power limiting (if necessary) is proposed to improve the stability of the allied system. The proposed strategies are verified by both software simulation and field commissioning.**

***Index Terms*—Control strategy optimization, islanded renewable power plants, stability, voltage source converter (VSC), AC system.**

I. Introduction

THE voltage source converter (VSC), which adopts fully-controlled power electronics, is capable of controlling active and reactive power independently. Since the VSC does not rely on AC systems to provide commutation voltage, there is no commutation failure when connected to weak AC systems [1], [2], even in islanded power systems such as islanded renewable power plants [3]-[7]. When connected to strong AC systems, the VSC can limit the short-circuit current and improve the transient stability of AC systems [8]-[10].

However, the operation characteristics are different in these cases, and traditional control strategies need to be optimized accordingly. When a VSC is connected to islanded renewable power plants, the traditional voltage/frequency (*V*/*f*) control is susceptible to power fluctuation disturbances. Meanwhile, if bipolar VSCs adopt the traditional *V*/*f* control, the system is prone to instability because the two converters independently control the same target. Moreover, the wide-band oscillation between the VSC and the renewable power plants poses significant risks. Because of the scale and complexity, the accurate simulation of renewable power plants is very challenging, which makes it difficult to measure the wide-band impedance characteristics in the frequency domain. The literature has mainly focused on the characteristics of renewable energy units, specifically on the low- or medium-frequency bands [11]-[14]. VSCs have fast response and flexible regulation capabilities, which can be adopted to reduce the transients under disturbances. However, when they are connected to strong AC systems via traditional control strategies, these capabilities are usually lost. On the other hand, when VSCs are connected to extremely weak AC systems, the allied system is likely to lose stability even under small disturbances [15]-[17].

This study optimizes the control strategies of VSCs connected to various types of AC systems. For the VSCs connected to islanded renewable power plants, the *V*/*f* droop control strategy is proposed to damp power fluctuation disturbance by adopting active power/frequency (P_s/*f*) and reactive power/voltage droop control strategies, which is vital for bipolar VSC control. In addition, a multi-branch impedance equivalent method for renewable power plants is proposed to accurately obtain the impedance characteristics of large-scale renewable power plants to prevent wide-band oscillations. For VSCs connected to strong AC systems, smart AC voltage and coordinated frequency transient control strategies are proposed. These strategies achieve three purposes: supporting voltage and frequency during transients, keeping the reactive power margin in a steady state, and providing coordinated frequency transient control for the AC systems connected with different converters. For the VSCs connected to weak AC systems, the control strategy of optimizing the inner-loop control parameter and limiting the outer-loop power (if necessary) is proposed to ensure the stability of the allied system. This strategy is based on the analysis of the relationship between the transmission capacity of the allied system and the system strength.

Manuscript received: June 4, 2020; accepted: September 14, 2020. Date of CrossCheck: September 14, 2020. Date of online publication: January 11, 2021.

Z. Liu and X. Guo (corresponding author) are with State Grid Corporation of China, Beijing 100031, China (email: zehong-liu@sgcc. com. cn; xianshanguo@sgcc.com.cn).

DOI: 10.35833/MPCE.2020.000352

II. Control Strategy Optimization for VSCs Connected to Islanded Renewable Power Plant

A. Control Strategy Optimization for Islanded System

When connected to islanded renewable power plants, the VSCs determine the AC voltage, and the renewable power plants determine the output power based on this AC voltage. The fluctuation of power causes constant disturbances. If the VSC adopts the traditional *V*/*f* control by setting a fixed AC voltage and frequency reference, the fluctuation cannot be properly damped, which may cause instability.

It is known that the system stability is based on the balance of the active and reactive power of the islanded system. Regarding the relationship between active power and frequency in the primary frequency regulation of synchronous generators [18], [19], the *V*/*f* droop control strategy is proposed, the characteristics of which are shown in Fig. 1. Differences in frequency and voltage references at the point of common coupling (PCC) are proportional to the differences in active and reactive power input to the PCC, respectively.

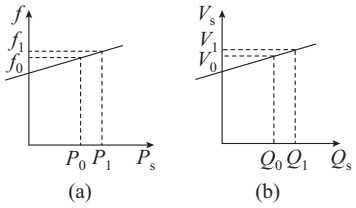

Fig. 1. Characteristics of droop control strategies. (a) P_s/f droop control strategy. (b) Reactive power/AC voltage (Q_s/V_s) droop control strategy.

During steady-state operation, the VSCs operate at P_0-f_0. Assume that active power input to PCC, denoted as P_s, increases to P_1 as the active power output from renewable power plants increases. According to the P_s/f droop characteristics shown in Fig. 1(a), the frequency reference of the control system is automatically revised from f_0 to f_1. That is, the VSC inputs more active power, whereas the renewable power units output less active power (if renewable power is capable of frequency regulation) to stabilize the system.

The balance of the reactive power of the islanded system is similar to that of the active power. During steady-state operation, the VSCs operate at Q_0-V_0. Assume that reactive power input to PCC, denoted as Q_s, increases to Q_1 when the active power input from the renewable power plants drops. According to the Q_s/V_s droop characteristics shown in Fig. 1(b), the AC voltage reference of the control system will be automatically revised from V_0 to V_1. That is, VSC consumes more reactive power, whereas the renewable power plants output less reactive power to stabilize the system.

Its control block based on the principle of *V*/*f* droop control is shown in Fig. 2, where PI stands for proportional-integral.

With the proposed control strategy, a collaborative control can be achieved for bipolar VSCs connected to islanded renewable power plants. If a traditional *V*/*f* control is adopted for bipolar VSCs, the system is likely to be unstable because the two converters control the same target independently. Another possible strategy is to set one pole to be the *V*/*f* control and the other pole to be the active power/reactive power (*P*/*Q*) control, but there are some disadvantages: ① since only one pole controls the AC voltage, the power of the pole in the *V*/*f* control is likely to reach its rating, resulting in a loss of the AC voltage controllability; ② since the pole reference in the *P*/*Q* control is generally maintained when the power from the renewable power plants is fluctuating, it is difficult to distribute the power optimally between the two poles; ③ when the pole in the *V*/*f* control is blocked because of a fault, the pole in the *P*/*Q* control will switch to *V*/*f* control, and the AC voltage will fluctuate.

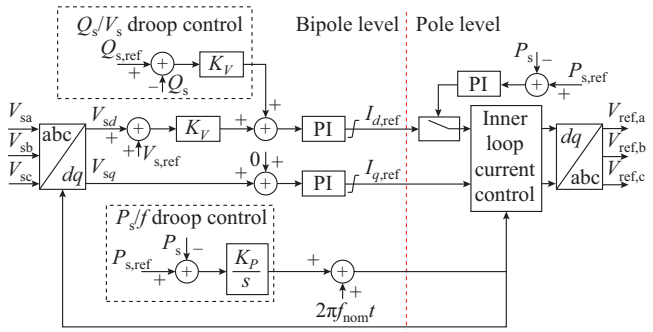

Fig. 2. *V*/*f* droop control block.

To adapt the proposed control strategy to the bipoles, a dominant pole is set to monitor the active and reactive power input to the converter station and to generate the total current references $I_{d,\mathrm{ref}}$ and $I_{q,\mathrm{ref}}$, which are divided into the current references for each pole. The inner loop is similar to the traditional control; thus, the details are omitted here.

B. Wide-band Oscillation Detection and Prevention when VSCs Connected to Islanded Renewable Power Plant

When the VSCs are connected to renewable power plants, there is a risk of wide-band oscillation. This is caused by the inherent time delay of the control system based on power electronics, low inertia of the renewable energy units, and critical AC transmission lines among other factors.

To detect wide-band oscillation, it is necessary to obtain the impedance characteristics of the renewable power plants based on frequency-domain impedance scanning. The first step should be to build a time-domain model for the renewable power plants. However, as there are a lot of equipment and AC lines in renewable power plants and the operation conditions are innumerable, it is difficult to perform time-domain simulation accurately and thoroughly.

Therefore, this paper proposes a multi-branch impedance equivalent method for renewable power plant simulation in the frequency domain. The typical topology of a renewable power plant is shown in Fig. 3(a). All the equipment, including renewable energy units, transformers, and transmission lines in the renewable power plant can be expressed as frequency-dependent impedances in the frequency domain. Thus, the equivalent circuit of the entire renewable power plant is obtained, as shown in Fig. 3(b). Then, the multi-branch impedance equivalent method is used to obtain the impedance of the entire renewable power plant as follows.

$$Z_{RP} = Z_T + Z_L + (Z_{p1} + Z_{t1} + Z_{l1}) \| (Z_{p2} + Z_{t2} + Z_{l2}) \| \ldots \| \left(Z_{pn} + Z_{tn} + Z_{ln} \right) \quad (1)$$

where Z_{RP}, Z_T, and Z_L are the impedance of the renewable power plant, high-voltage transformer, and high-voltage AC line, respectively; and Z_{pi}, Z_{ti}, and Z_{li} are the impedance of the renewable energy unit, low-voltage transformer, and low-voltage AC line on the i^{th} branch ($1 \le i \le n$), respectively.

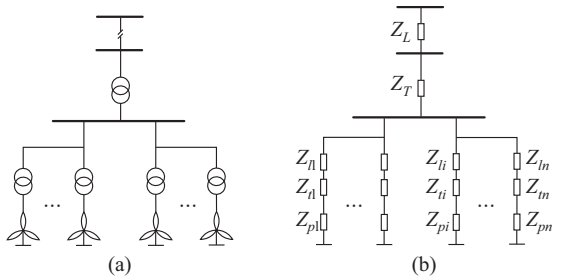

Fig. 3. Typical topology and equivalent circuit of a renewable power plant. (a) Typical topology. (b) Equivalent circuit.

It is difficult to obtain analytical expressions for the impedance of the renewable energy unit in (1), as it is highly nonlinear. However, the impedance characteristics of a single renewable energy unit can be obtained by impedance scanning.

Taking a typical small-scale wind farm including four doubly-fed induction generators as an example, the characteristics of the impedance Z obtained with the proposed multi-branch impedance equivalent method is verified by comparing it with direct impedance scanning method, as shown in Fig. 4. It can be seen that the impedance characteristics based on the two methods are consistent in the entire frequency band.

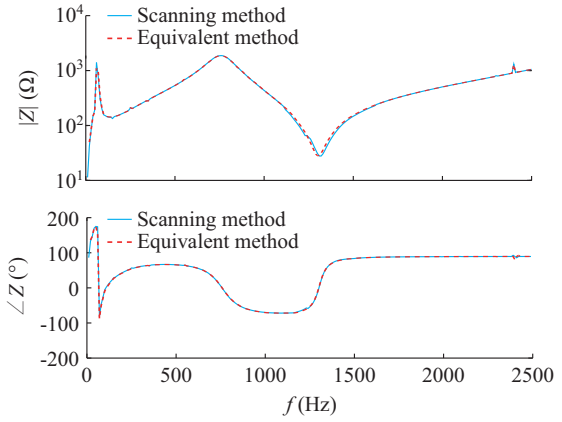

Fig. 4. Verification of multi-branch impedance equivalent method.

On the island, the VSC converters are the only voltage source for the entire AC system, and the renewable power plants output the power by tracking the AC voltage. Thus, the equivalent model of the island is obtained [20], as shown in Fig. 5. The allied system is unstable if the following criteria are satisfied:

$$\begin{cases} |Z_{VSC} + Z_{RP}| = 0 \\ \mathrm{Re}(Z_{VSC}) + \mathrm{Re}(Z_{RP}) \le 0 \end{cases} \quad (2)$$

where Z_{VSC} is the equivalent impedance of VSC.

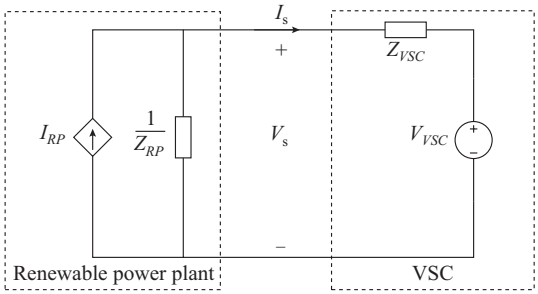

Fig. 5. Equivalent circuit of VSC connected to renewable power plants.

C. Verification of Proposed Control Strategies

To analyze the characteristics of the proposed strategies, a real-time simulation model based on the Zhangbei four-terminal DC grid project of China is built. The control strategies under comparison are listed in Table I.

TABLE I
TWO CONTROL STRATEGIES FOR BIPOLAR CONVERTER STATION

Pole	Strategy 1	Strategy 2
P1	*V*/*f* control	*V*/*f* droop control
P2	*P*/*Q* control	*V*/*f* droop control

A permanent single-phase-to-ground fault on a transmission line of an AC inverter station is set at $t = 2.0$ s. According to the principle of the transmission line protection, the circuit breakers at both ends of the transmission line trip at $t = 2.2$ s, reclose at $t = 3.2$ s, and trip again at $t = 3.4$ s.

When the fault occurs, the inverter decreases the output power to avoid overcurrent, while the rectifier maintains the input power, and the surplus power stored in the VSC system. Thus, the DC voltage V_{dc} increases as the surplus power accumulates. Since both poles suffer from DC overvoltage, AC choppers, which consume all the active power from the renewable power plants, are switched on. Then, the AC choppers are switched on and off according to the DC voltage levels.

As shown in Fig. 6(a), if strategy 1 is adopted, as the active power reference of P2 is maintained, P2 draws active power from P1 to follow the power reference. Thus, there is still a critical DC overvoltage in P2.

As shown in Fig. 6(b), if strategy 2 is adopted, both poles decrease the input power as the bipolar input power decreases to almost zero after switching on the AC choppers. Thus, the DC overvoltage vanishes immediately.

According to the topology and parameters of the renewable power plants to be put into operation, the equivalent impedance characteristics of the power plants are obtained using the multi-branch impedance equivalent method. The impedance characteristics of the VSC are obtained with direct impedance scanning. As shown in Fig. 7, with the correction of the control parameters in the VSC and the renewable power plants, the impedance characteristics of the allied system meet the stability criterion.

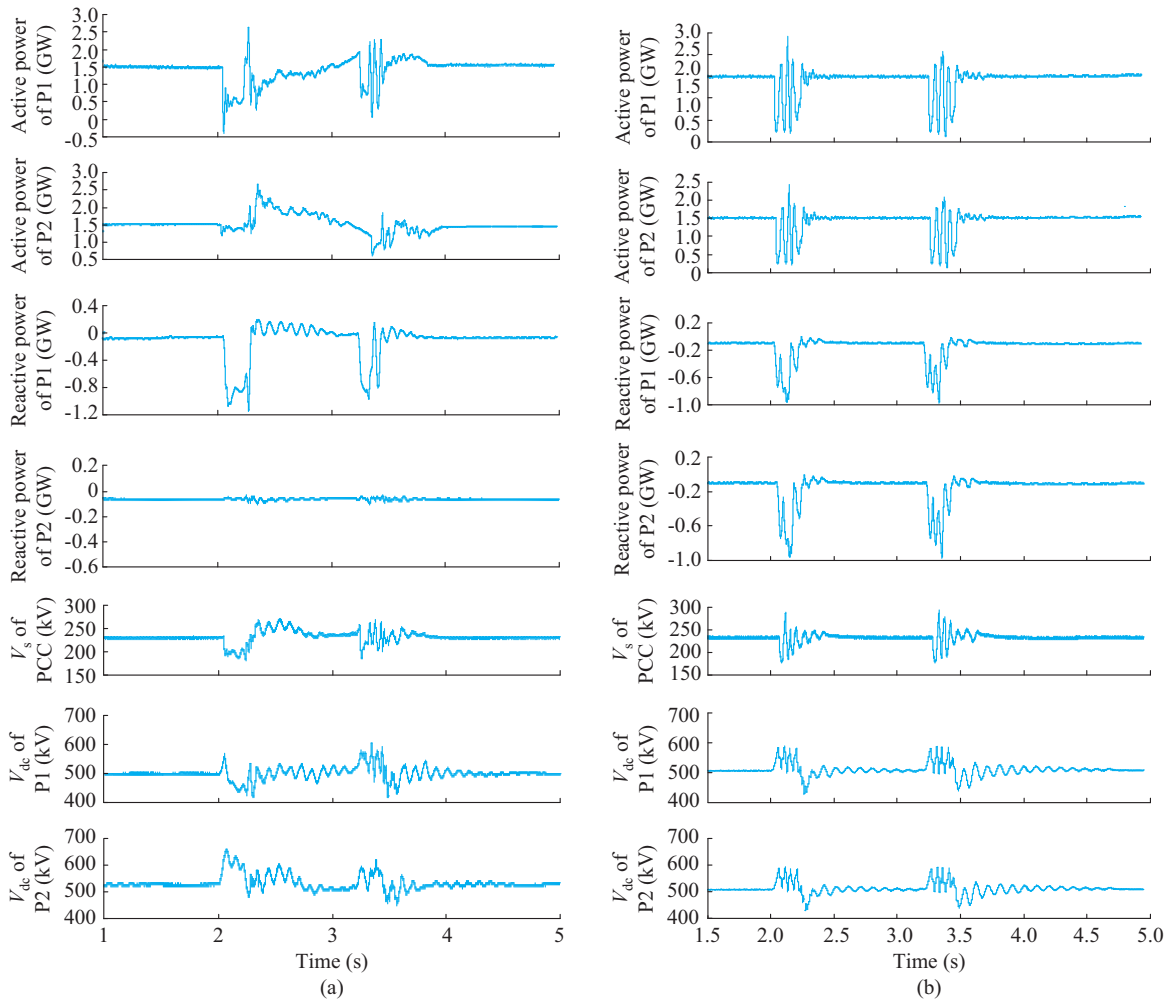

Fig. 6. Comparison of two control strategies after single-phase-to-ground fault. (a) Strategy 1. (b) Strategy 2.

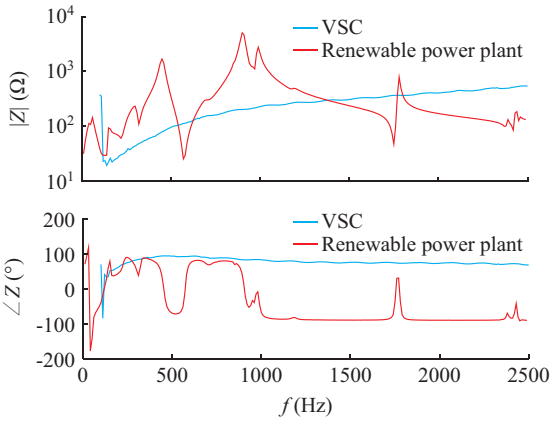

Fig. 7. Impedance characteristics of VSC and renewable power plant.

III. Voltage and Frequency Control Strategy Optimization for VSCs Connected to Strong AC Systems

A. Smart AC Voltage Transient Control with Steady-state Reactive Power Resetting Functions

Compared with common reactive power regulation equipment in AC systems, VSCs respond much faster to AC voltage fluctuations. As the reactive power provided by the VSC accumulates, it is likely to reach the power rating, leaving little margin for the subsequent transients [21].

Thus, a smart AC voltage transient control with a steady-state reactive power resetting function is proposed, and its control blocks are shown in Fig. 8. The proposed control strategy sets a dead zone for the AC voltage in terms of the strength of the AC systems and the adjustment requirements such as preventing the VSC from participating in the steady-state regulation of the AC voltage. The three states for the voltage controller are as follows.

1) During steady-state operation, the AC voltage fluctuates within the dead zone ΔV_{db}, and the AC voltage controller produces no responses other than those for voltage regulation of the devices in the AC system. Note that the corrected voltage deviation ΔV is kept at zero in this state.

2) With large disturbances, the AC voltage fluctuates beyond the dead zone, and the AC voltage controller responds immediately to stabilize the transient AC voltage. During this state, ΔV is set as the deviation of the measured AC voltage from the limit value. Since the parameter of resetting loop k_{pb} in the resetting loop is much smaller than k_p in the PI loop [22], the reactive power reference $Q_{s,ref}$ is mainly determined by the PI loop, as shown in Fig. 8. It should be

noted that, if the AC voltage remains beyond the dead zone after VSC reaches the reactive power rating, the reactive power of the VSC is maintained afterwards.

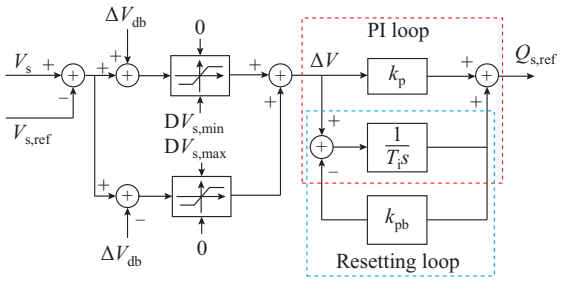

Fig. 8. AC voltage control block with resetting loop.

3) When the AC voltage returns within the dead zone, the AC voltage controller enters the steady-state reactive power resetting process, reserving the reactive power capacity for the consequent transients. During this state, ΔV returns to zero. The output of the proportional loop is zero, and the reactive power reference $Q_{s,ref}$ is mainly determined by the resetting loop, as shown in Fig. 8.

B. Coordinated Frequency Transient Control

While common in the literature, frequency transient control in one converter will deteriorate the frequency of AC systems connected to the other converters owing to the active power coupling between the converters in a VSC based high-voltage direct current (VSC-HVDC) system. Take a two-terminal VSC-HVDC system as an example, the control block of the coordinated frequency transient control is shown in Fig. 9. The proposed control strategy sets a frequency dead zone, similar to that of the smart AC voltage transient control. Meanwhile, the frequency fluctuations of both the rectifier and inverter are considered at the same time due to the active power coupling between converters. The two states for the frequency controller are as follows.

1) During steady-state operation, the frequencies on both AC systems (f_R and f_I) fluctuate within the dead zones (Δf_{Rdb} and Δf_{Idb}). The frequency controllers produce no responses other than those for the generators in the AC systems. Note that the corrected frequency deviations Δf_R and Δf_I are kept at zero in this state.

2) With large disturbances, f_R (or f_I) fluctuates beyond the dead zone, and the frequency controller responds immediately and participates in adjusting the frequency of the AC system. During this state, f_R (or f_I) is set as the deviation of the measured frequency from the limit value. After the P_s/f droop control is carried out, the active power ramp $\Delta P_{s,ref,R}$ (or $\Delta P_{s,ref,I}$) is obtained and added to (or subtracted from) the active power reference $P_{s,ref}$ of VSC to damp the frequency fluctuations.

C. Verification of Proposed Control Strategies

To verify the response characteristics of the proposed control strategies, a real-time simulation model based on the Chongqing-Hubei back-to-back interconnection DC project of China is built, the topology of which is shown in Fig. 10.

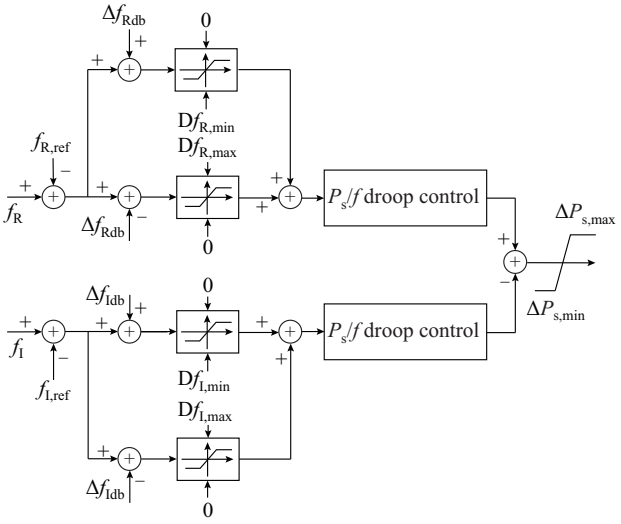

Fig. 9. Coordinated frequency transient control block.

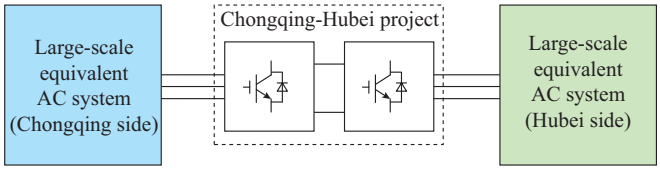

Fig. 10. Topology of Chongqing-Hubei back-to-back interconnection DC project of China and connected AC system.

Table II shows that strategy 2 resets after the disturbance while maintaining the dynamic response characteristics. Table III shows that strategy 2 can support frequency at one side while maintaining acceptable frequency characteristics at the other side after the disturbance.

TABLE II
COMPARISON OF AC VOLTAGE CONTROL CHARACTERISTICS

Strategy	Voltage step test	Response time (ms)	Reactive power reference after step (Mvar)
Strategy 1	525 kV → 545 kV	956	187 (output)
	545 kV → 505 kV	973	0
Strategy 2	525 kV → 545 kV	638	335 (input)
	545 kV → 505 kV	650	0

TABLE III
COMPARISON OF FREQUENCY CONTROL CHARACTERISTICS WHEN SINGLE LINE TRIP FAULT OCCURS AT HUBEI SIDE

Terminal	Frequency disturbance (Hz)	
	Strategy 1	Strategy 2
Hubei side	0.08	0.15
Chongqing side	0.51	0.24

IV. CONTROL OPTIMIZATION FOR VSCS CONNECTED TO WEAK AC SYSTEMS

A. Control Strategy Optimization for Weak AC System

Compared with line-commutated converters (LCCs), VSCs

are suitable for connecting weak AC systems due to the following considerations.

1) LCCs adopt semi-controlled power electronics such as thyristors, and the AC system provides the commutation voltage. Thus, there is a risk of commutation failure for LCCs connected to weak AC systems. VSCs adopt fully-controlled power electronics such as insulated gate bipolar transistors (IGBTs), thereby avoiding any commutation failure irrespective of the AC system strength.

2) The switching on and off of AC filters in LCC stations cause disturbances to weak AC systems, whereas VSC can support the AC voltage of a weak system. Thus, an AC system connected with an LCC is generally defined as a weak system if the short-circuit ratio (SCR) is below 3.0 [23], [24]. On the other hand, an AC system connected with a VSC is generally defined as a weak system if the SCR is below 2.0 [25].

However, the stability margin of the allied system of the VSCs connected to weak AC systems declines with the connected AC system strength, and the VSC control system needs to be optimized. The equivalent circuit of the VSC connected to the AC system is shown in Fig. 11.

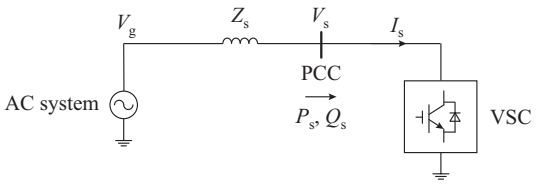

Fig. 11. Equivalent circuit of VSC connected to AC system.

The active power transmitted to the PCC P_s is denoted as:

$$P_s = -V_s^2 \frac{R_s}{|Z_s|^2} + \frac{V_s V_g}{|Z_s|} \cos(\delta - \phi) \tag{3}$$

where V_g is the magnitude of the equivalent AC system voltage; Z_s is the equivalent AC system impedance, with R_s being its real component; δ is the angle that V_g leads V_s; and ϕ is the impedance angle of the AC system.

The SCR is denoted as [25]:

$$SCR = \frac{S_s}{P_{dcN}} = \frac{V_s^2}{|Z_s|} \frac{1}{P_{dcN}} = \frac{1}{|Z_s^*|} \tag{4}$$

where S_s is the short-circuit power at the PCC; P_{dcN} is the nominal active power of the converter station; and * represents the per-unit value of the corresponding variables.

The per-unit power limitation $P_{s,max}^*$ obtained from (3) and (4) is:

$$P_{s,max}^* = SCR \cdot \left(\frac{V_g^*}{V_s^*} - \frac{R_s^*}{|Z_s^*|} \right) \tag{5}$$

From (5), we can observe that the active power transmitted to the PCC is related to V_s, V_g, and Z_s when ignoring the influence of the VSC control characteristics. If $\phi = 80°$ and $V_s^* = V_g^* = 1.0$ p.u., the lower limitation of SCR is 1.21.

Thus, ignoring the VSC control characteristics, the input active power to the converter station is limited by the AC system strength. When the SCR is below the lower limitation of SCR, the allied system is not stable.

Then, the influence of the VSC control system is further investigated. The *dq*-domain control strategy is widely adopted in VSC-HVDC systems. The phase angle of the PCC voltage is obtained by a phase-locked loop (PLL):

$$\begin{cases} V_{sd} = V_s \cos(\theta - \theta_{PLL}) \\ V_{sq} = V_s \sin(\theta - \theta_{PLL}) \end{cases} \tag{6}$$

where θ is the phase angle of the PCC voltage V_s; θ_{PLL} is the output of the PLL; and V_{sd} and V_{sq} are the *d*-axis and *q*-axis components of V_s, respectively.

In the *dq*-domain, P_s and Q_s can be written as:

$$\begin{cases} P_s = V_{sd} I_{sd} + V_{sq} I_{sq} \\ Q_s = V_{sd} I_{sq} - V_{sq} I_{sd} \end{cases} \tag{7}$$

where I_{sd} and I_{sq} are the *d*-axis and *q*-axis components of PCC current I_s, respectively.

If the PLL can track the phase angle of V_s accurately, V_{sq} is equal to zero. Thus, (7) can be rewritten as:

$$\begin{cases} P_s = V_{sd} I_{sd} \\ Q_s = V_{sd} I_{sq} \end{cases} \tag{8}$$

With P_s and Q_s being proportional to I_{sd} and I_{sq}, respectively, the active and reactive power decoupling control can be achieved in the VSCs. For VSCs connected to strong AC systems, the PCC voltage is stable and the PLL can track the phase accurately to realize decoupling control.

As the strength of the AC system decreases, the PCC voltage becomes increasingly susceptible to fluctuations, which makes it difficult for the PLL to track the PCC voltage phase accurately; that is, $V_{sq} \neq 0$. Moreover, P_s and Q_s are both related to I_{sd} and I_{sq}, and *dq* axis decoupling cannot be achieved, and this deteriorates the operation conditions of the VSCs. If the control system is not optimized, it may cause instability.

An optimized control strategy of the VSC is proposed to track the PCC voltage quickly, which benefits the PLL control and decoupling control, as illustrated in Fig. 12. Since the strength of the AC system decreases, the voltage disturbance ΔV caused by the same current disturbance ΔI increases. Therefore, it is necessary to increase the voltage step response $\Delta V_{control}$ to compensate for the voltage disturbance ΔV. Thus, the allied system is stabilized. Since the inner-loop PI control functions, denoted as G_{PI}, reflect the relationship between current disturbance and voltage step response, for a faster response than the outer-loop control, it is an effective measure to increase the proportional coefficient k_{pi} in the inner-loop control. However, if k_{pi} is excessively high, the poor damping characteristics of the VSC may lead to high-frequency oscillation.

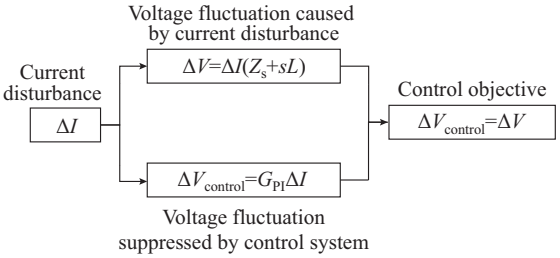

Fig. 12. Relationship between voltage disturbance and voltage step response of VSC.

Generally speaking, VSCs run with strong AC systems under normal conditions. However, when nearby electrical equipment or transmission lines are tripped, the VSCs may be connected to weak AC systems. In this case, the VSCs cannot accurately identify the change in the AC system strength by merely monitoring the voltage and current at the PCC. Thus, it is necessary to install a system-strength identifier to monitor the operation status of the nearby electrical equipment and transmission lines and identify the weak AC systems in time. When the AC systems becomes weak, the converter station receives the signal sent by the system-strength identifier, and the control system switches the controller parameters and power reference (if necessary) to ensure the stability of the allied system.

B. Verification of Proposed Control Strategy

Based on the above model of the Chongqing-Hubei project, a permanent 3-phase-to-ground fault is set on one of the 500 kV AC lines connected to the converter at the Chongqing side, with the connected AC system becoming weak after the trip.

Then, the VSC attempts to recover the power with the ramping current causing a large voltage disturbance. The allied system loses stability after several attempts by the VSC control system to recover the power, as shown in Fig. 13(a), where $V_{s,rms}$ is the root mean square of PCC voltage.

To solve this problem, a weak system signal from the system strength identifier is sent to the VSC after the trip, with the following measures taken to stabilize the allied system: ① the inner-loop control parameters are switched; ② the power reference, which exceeds the power limitation, is decreased. The transients with the proposed strategy are shown in Fig. 13(b).

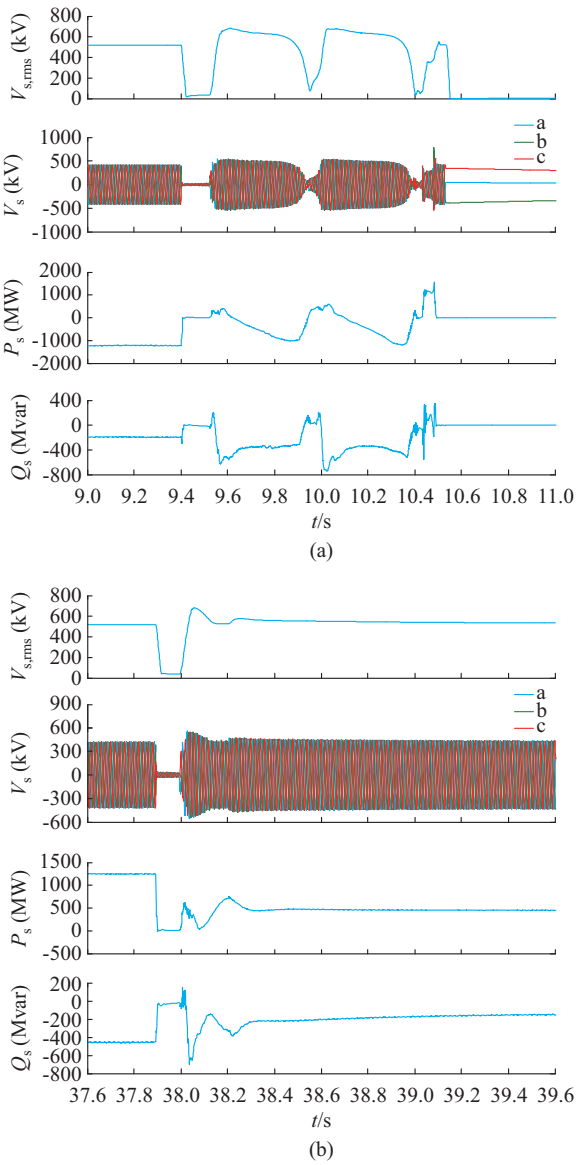

Fig. 13. Transients after fault. (a) Original transients after fault. (b) Transients after fault with optimization.

V. CONCLUSION

This study optimizes the control strategies of VSCs connected to various types of AC systems.

1) For VSCs connected to islanded renewable power plants, the *V*/*f* droop control strategy is proposed to damp power fluctuation disturbance by adopting P_s/f and reactive power/voltage droop control strategies, which is vital for bipolar VSC control. Then, a multi-branch impedance equivalent method for renewable power plants is proposed to accurately obtain the impedance characteristics of large-scale renewable power plants to prevent wide-band oscillations.

2) For VSCs connected to strong AC systems, smart AC voltage and coordinated frequency transient control strategies are proposed, which achieve three purposes: supporting voltage and frequency during transients, maintaining reactive power margin in a steady state, and providing coordinated frequency transient control for AC systems connected with different converters.

3) For VSCs connected to weak AC systems, the control strategy of inner-loop control parameter optimization and limiting outer-loop power (if necessary) is proposed to ensure the stability of the allied system based on the analysis of the relationship between the transmission capacity of the allied system and the system strength.

The control strategies proposed in this paper have been adopted in the Chongqing-Hubei back-to-back interconnection DC project and Zhangbei 4-terminal DC grid project and validated by both software simulation and field commissioning.

REFERENCES

[1] S. Song, R. Guo, F. Chen *et al.*, "A real-time power flow optimal control method for hybrid AC/DC power systems with VSC-HVDC," in *Proceedings of 2016 International Conference on Smart Grid and Electrical Automation (ICSGEA)*, Zhangjiajie, China, Aug. 2016, pp. 26-30.

[2] X. Yu, T. Yang, K. Cao *et al.*, "Analysis of influence factors on the transmission capability of the Yu-E back-to-back VSC-HVDC south channel," in *Proceedings of 2019 IEEE Innovative Smart Grid Technologies - Asia (ISGT Asia)*, Chengdu, China, Mar. 2019, pp. 291-295.

[3] Y. Li, H. Liu, C. Liu *et al.*, "Study on AC-side dynamic braking-based fault ride-through control for islanded renewable energy system with grid-connected VSC-HVDC transmission," in *Proceedings of 2017 Chinese Automation Congress (CAC)*, Jinan, China, Sept. 2017, pp. 6108-6111.

[4] D. Kong and X. Zhang, "Transient stability analysis and optimal coor-

dinated control of multi-terminal VSC-HVDC based offshore wind farms," in *Proceedings of the IET Conference on Renewable Power Generation (RPG 2011)*, Edinburgh, UK, Sept. 2011, pp. 1-8.
[5] D. V. Hertem, O. Gomis-Bellmunt, and J. Liang, *HVDC Grids: for Offshore and Supergrid of the Future*. Piscataway: Wiley, 2016, pp. 1-7.
[6] L. Wang, Y. Huang, A. V. Prokhorov *et al*., "Integration of a DFIG-based offshore wind farm and a PMSG-based offshore wind farm connected to a power grid through a VSC-HVDC link," in *Proceedings of 2018 IEEE Industry Applications Society Annual Meeting (IAS)*, Portland, USA, Sept. 2018, pp. 1-9.
[7] G. Shi, J. Zhang, X. Cai *et al*., "Decoupling control of series-connected DC wind turbines with energy storage system for offshore DC wind farm," in *Proceedings of 2016 IEEE 7th International Symposium on Power Electronics for Distributed Generation Systems (PEDG)*, Vancouver, Canada, Jun. 2016, pp. 1-6.
[8] O. Gomis-Bellmunt, J. Sau-Bassols, E. Prieto-Araujo *et al*., "Flexible converters for meshed HVDC grids: from flexible AC transmission systems (FACTS) to flexible DC grids," *IEEE Transactions on Power Delivery*, vol. 35, no. 1, pp. 2-15, Feb. 2020.
[9] D. Jovcic and K. Ahmed, *High Voltage Direct Current Transmission: Converters, Systems and DC Grids*. Chichester: Wiley, 2015, pp. 123-139.
[10] S. Teng, G. Li, X. Song *et al*., "A novel method for VSC-HVDC electromechanical transient modeling and simulation," in *Proceedings of 2012 Power Engineering and Automation Conference*, Wuhan, China, Sept. 2012, pp. 1-4.
[11] H. Liu, X. Xie, J. He *et al*., "Subsynchronous interaction between direct-drive PMSG based wind farms and weak AC networks," *IEEE Transactions on Power Systems*, vol. 32, no. 6, pp. 4708-4720, Feb. 2017.
[12] M. Céspedes and J. Sun, "Modeling and mitigation of harmonic resonance between wind turbines and the grid," in *Proceedings of 2011 IEEE Energy Conversion Congress and Exposition*, Phoenix, USA, Sept. 2011, pp. 2019-2116.
[13] I. Vieto and J. Sun, "Sequence impedance modeling and converter-grid resonance analysis considering DC bus dynamics and mirrored harmonics," in *Proceedings of 2018 IEEE 19th Workshop on Control and Modeling for Power Electronics (COMPEL)*, Padua, Italy, Jun. 2018, pp. 1-9.
[14] Y. Xu, H. Nian, and J. Sun, "Cross coupling of grid-connected inverter impedance over frequency phenomena, effects and modeling" in *Proceedings of the 15th Wind Integration Workshop ENERCON Energy for the World*, Vienna, Austria, Nov. 2016, pp. 1-8.
[15] J. Lyu, X. Cai, and M. Molinas, "Frequency domain stability analysis of MMC-based HVDC for wind farm integration," *IEEE Journal of Emerging and Selected Topics in Power Electronics*, vol. 4, no. 1, pp. 141-151, Feb. 2016.
[16] M. Amin, M. Molinas, and J. Lyu, "Oscillatory phenomena between wind farms and HVDC systems: the impact of control," in *Proceedings of 2015 IEEE 16th Workshop on Control and Modeling for Power Electronics*, Vancouver, Canada, Jul. 2015, pp. 1-8.
[17] K. Ilves, A. Antonopoulos, S. Norrga *et al*., "Steady-state analysis of interaction between harmonic components of arm and line quantities of modular multilevel converters," *IEEE Transactions on Power Electronics*, vol. 27, no. 1, pp. 57-68, Aug. 2012.
[18] C. Lee, C. Chu, and P. Cheng, "A new droop control method for the autonomous operation of distributed energy resource interface converters," in *Proceedings of the Energy Conversion Congress and Exposition (ECCE)*, Atlanta, USA, Sept. 2010, pp. 12-16.
[19] W. Yao, M. Gao, R. Zheng *et al*., "Study on the impact of the complex impedance on the droop control method for the parallel inverters," in *Proceedings of the Applied Power Electronics Conference and Exposition (APEC)*, Palm Springs, USA, Feb. 2010, pp. 21-25.
[20] F. Liu, J. Liu, H. Zhang *et al*., "Stability issues of Z + Z type cascade system in hybrid energy storage system (HESS)," *IEEE Transactions on Power Electronics*, vol. 29, no. 11, pp. 5846-5859, Aug. 2014.
[21] Y. Amirnaser and R. Iravani, *Voltage-sourced Converters in Power Systems*. New Jersey: John Wiley & Sons, 2010, pp. 205-242.
[22] K. J. Astrom and T. Hagglund, *PID Controllers: Theory, Design, and Tuning*. Charlotte: The Instrumentation, Systems, and Automation Society, 1995, pp. 120-196.
[23] *IEEE Guide for Planning DC Links Terminating at AC Locations Having Low Short-circuit Capacities*, IEEE Standard 1204-1997, 1997.
[24] P. Kunder, *Power System Stability and Control*. New York: McGraw-Hill Professional, 1994, pp. 528-535.
[25] H. Chao, "Improving fault recovery performance of an HVDC link with a weak receiving AC system by optimization of DC controls," in *Proceedings of 2018 International Conference on Power System Technology (POWERCON)*, Guangzhou, China, Nov. 2018, pp. 4474-4479.

Zehong Liu received the B.S. degree in electrical engineering from Hunan University of China, Changsha, China, in 1981, and the M.S. degree in electrical engineering from China Electric Power Research Institute, Beijing, China, in 1984. He has been working on high-voltage direct current (HVDC) for more than 30 years. He is the Senior Member of IEEE, Member of AG1/B4 of CIGRE, and Senior Member of Chinese Society for Electrical Engineering (CSEE). He almost experienced all R&D and almost all projects in China including ±500 kV and ±800 kV HVDC. Currently, he is mainly working on the R&D and project management of ±1100 kV HVDC projects in State Grid Corporation of China. His research interest mainly focuses on ultra-high-voltage direct current (UHVDC) transmission technologies.

Xianshan Guo received the B.S. degree in electrical engineering from Huazhong University of Science and Technology, Wuhan, China, in 1994, and the M.S degree in energy engineering from Huazhong University of Science and Technology, in 1997. He has been working on design of HVDC project and has attended almost all the design of HVDC project in State Grid Corporation of China. His research interest mainly focuses on DC transmission technologies.